Journal of Microbiological Methods 132 (2017) 46–55

Contents lists available at ScienceDirect

Journal of Microbiological Methods

journal homepage: www.elsevier.com/locate/jmicmeth

Visualization of *Aspergillus fumigatus* biofilms with Scanning Electron Microscopy and Variable Pressure-Scanning Electron Microscopy: A comparison of processing techniques

Lydia-Marie Joubert [a,*], Jose AG Ferreira [b,c,1], David A Stevens [b,c], Hasan Nazik [b,c,2], Lynette Cegelski [d]

[a] Cell Sciences Imaging Facility, Stanford University School of Medicine, Stanford, CA, USA
[b] Division of Infectious Diseases and Geographic Medicine, Stanford University, Stanford, CA, USA
[c] California Institute for Medical Research, San Jose, CA, USA
[d] Department of Chemistry, Stanford University, Stanford, CA, USA

ARTICLE INFO

Article history:
Received 26 August 2016
Received in revised form 6 November 2016
Accepted 6 November 2016
Available online 9 November 2016

Keywords:
Aspergillus fumigatus
Biofilms
Scanning Electron Microscopy
Variable Pressure-SEM
Processing techniques

ABSTRACT

Aspergillus fumigatus biofilms consist of a three-dimensional network of cellular hyphae and extracellular matrix. They are involved in infections of immune-compromised individuals, particularly those with cystic fibrosis. These structures are associated with persistence of infection, resistance to host immunity, and antimicrobial resistance. Thorough understanding of structure and function is imperative in the design of therapeutic drugs. Optimization of processing parameters, including aldehyde fixation, heavy metal contrasting, drying techniques and Ionic Liquid treatment, was undertaken for an ultrastructural approach to understand cellular and extracellular biofilm components. Conventional and Variable Pressure Scanning Electron Microscopy were applied to analyze the structure of biofilms attached to plastic and formed at an air-liquid interface.

1. Introduction

A biofilm can be defined as a community of microbial cells surrounded by a self-produced polymeric matrix, which facilitates adhesion among cells and/or to other surfaces or interfaces (Costerton et al., 1995; Lappin-Scott et al., 2014; Donlan, 2002). *Aspergillus fumigatus* has recently been shown to form three-dimensional assemblies, 10–200 μm thick, and with typical biofilm characteristics (Muller et al., 2011; Beauvais et al., 2007, 2009, 2014; Kaur and Singh, 2014; Mowat et al., 2007). *A. fumigatus* is frequently isolated from cystic fibrosis (CF) patients, and *Aspergillus* biofilms contribute to virulence in CF and invasive pulmonary aspergillosis (Speirs et al., 2012; De Vrankrijker et al., 2011; Chotirmall et al., 2014; Polke et al., 2015). *A. fumigatus* biofilms are of increasing biomedical interest due to their association with chronic and lethal infections, notably in immunosuppressed patients, and their increased resistance to antifungal agents (Santos, 2015). Fungal biofilms also colonize abiotic surfaces and contribute to biofilm-related infections of implanted medical devices, e.g. catheters, pacemakers, prosthetic devices, and lenses (Nobile and Johnson, 2015; Yousif et al., 2015, Kojic and Darouiche, 2004). An estimated 80% of all infections in the USA are associated with microbial biofilms (Fox and Nobile, 2012). Biofilms are a significant cause of morbidity and mortality in the clinic and additionally impact the health care system through escalating costs of treating chronic biofilm-associated infections.

Understanding the composition and ultrastructure of microbial biofilms is imperative in understanding function and to developing strategies to control biofilm formation. The extracellular matrix (ECM) includes the extracellular polymeric substances (EPS) that surround resident cells, and serves as a physical and chemical barrier to antimicrobials, competitors and immune responses (Manavathu et al., 2014; Xiao et al., 2012). The ECM also contributes to biofilm hydration and nutrient transport (Flemming et al., 2007), and provides the mechanical integrity to withstand turbulent fluid forces and retain biofilm structure. Biofilms can be multi-species and can change over time, where the biofilm can accumulate 'immigrant' microbes, altering the structure and function of the community. Characterization of the biofilm extracellular

Abbreviations: BSE, Backscattered Electron; CF, cystic fibrosis; CPD, critical point drying; ECM, extracellular matrix; EPS, extracellular polymeric substances; ET, Everhart-Thornley; FESEM, Field Emission Scanning Electron Microscopy; GA, glutaraldehyde; HMDS, hexamethyldisilazane; NMR, Nuclear Magnetic Resonance; OsO4, osmium tetroxide; PBS, phosphate-buffered saline; PFA, paraformaldehyde; SE, Secondary Electron; SEM, Scanning Electron Microscopy; SNR, Signal to Noise Ratio; VP-SEM, Variable Pressure-SEM.

* Corresponding author.
E-mail address: lydiaj@stanford.edu (L.-M. Joubert).
[1] Current address: School of Medicine, Faculdade da Saúde e Ecologia Humana-FASEH, Vespasiano, Brazil.
[2] Permanent affiliation: Department of Medical Microbiology, Istanbul University, Turkey.

http://dx.doi.org/10.1016/j.mimet.2016.11.002
0167-7012/

matrix, in addition to its cellular organization, is therefore important for a holistic analysis of biofilm structure-function relationships.

It has been shown in vitro that *Aspergillus* produces an extracellular matrix (ECM) with typical biofilm characteristics under static and shaken, submerged conditions (Muller et al., 2011). In a recent study, we implemented a top-down approach to examine the composition and architecture of the ECM produced by *A. fumigatus* (Reichhardt et al., 2015) using solid-state Nuclear Magnetic Resonance (NMR) and Scanning Electron Microscopy (SEM). The top-down NMR approach was used to measure and quantify fundamental chemical parameters of the intact ECM. The NMR analysis determined that the ECM of *A. fumigatus* biofilms grown in RPMI 1640 nutrient medium was composed of predominantly polysaccharide and proteins, accounting for ~80% of the ECM, with lipids and aromatic compounds contributing to the remaining 20%. NMR is a powerful tool in the analysis of ECM chemical composition (Cegelski, 2015; Reichhardt et al., 2016). Yet, SEM is uniquely suited to the analysis of biofilm architecture and ultrastructure. SEM analysis of the biofilm samples in the NMR study showed biofilm hyphae as being densely packed and surrounded by tightly woven webs of ECM, with some ECM serving to glue hyphae together into a contiguous network.

In the present work, we report on the development of optimal protocols for examining *A. fumigatus* biofilms by SEM and the new details that are observed using SEM. Electron microscopy generally introduces some artifacts in structure, and interpretation of ultrastructure includes cognition of the physico-chemical influence of each step of processing protocols. The protocol of choice is therefore mostly optimized for a specific feature that is under investigation (Bozzola and Russell, 1999; Joubert et al., 2015). Stabilization of proteins through aldehyde cross-linking, with post-fixation of lipids via osmium tetroxide (OsO_4), generally maintains ultrastructure (Hayat, 2000; Bozzola and Russell, 1999), while preservation of fine features is attempted through critical point drying (CPD) or hexamethyldisilazane (HMDS) as a final drying agent (Bray et al., 1993). In biofilms, some loss of 3D architecture is commonly associated with dehydration required for conventional SEM (Alhede et al., 2012). Variable Pressure (VP)-SEM enables the observation of biofilms in their natural hydrated state (Weimer et al., 2006; Priester et al., 2007; Weber et al., 2014), with the ECM often observed as a gel-like film. However, resolution is compromised under extended pressures and through the inclusion of water vapor and gas in the specimen chamber; cellular features are hidden under the electron-dense film, which may blanket hydrated cells. Ruthenium Red has been described as a suitable contrasting agent in hydrated biofilms (Priester et al., 2007; Weber et al., 2014), and recently Ionic Liquids (IL) have been reported to improve imaging of hydrated biofilms by preserving their natural in situ 3D architecture (Asahi et al., 2015; Joubert and McDonald, 2016). OsO_4 has also been described as a contrasting agent to localize cells growing on hydrogels, by providing differential binding to lipids, which are generally located in cell membranes and cellular compartments (Joubert, 2009, 2012). Cryo-SEM techniques have been applied in various approaches from cryo-fixation by plunge-freezing and lyophilization (Villena et al., 2010), to freezing with liquid nitrogen and ethane followed by cryo-SEM imaging of the frozen-hydrated biofilms (Wu et al., 2014; Beauvais et al., 2007). Wu et al. (2014) aptly point out that different cryo-preparation methods give rise to markedly different biofilm morphologies. Here we focus on ambient temperature SEM, and include cryo-processing as plunge-freezing with liquid N_2, followed by freeze drying for conventional FESEM.

In this study, we share our observations on the ultrastructural component of biofilm development (ECM and cellular) using conventional SEM, Field Emission SEM (FESEM) and VP-SEM. We investigated the effect of processing techniques and reagents on the ultrastructure of the cellular mycelium and ECM of two modes of biofilm growth of *A. fumigatus*: growth on a solid substrate and growth in suspension at the liquid-air interface. Processing parameters included: (1) time in primary aldehyde fixatives, (2) the inclusion of OsO_4 as a secondary fixative, (3) final drying through CPD or HMDS, (4) hydrated structure analysis with VP-SEM, (5) inclusion of Ruthenium Red as contrasting agent for hydrated biofilms (6) application of Ionic Liquid as alternative to conventional processing, and (6) cryofixation and lyophilization for FESEM analysis. We also (7) introduce Ruthenium tetroxide (RuO_4) as alternative contrasting reagent to visualize hydrated biofilms using VP-SEM. We analyzed samples with these varying parameters using a combination of two scanning electron microscopes: a VP-SEM and a Field Emission SEM (FESEM). We provide our observations and conclude with recommendations for *A. fumigatus* biofilm analysis by SEM.

2. Material and methods

A. fumigatus biofilms were grown in RPMI 1640 culture medium on 12 mm circular plastic rotating bioreactor disks or as a floating biofilm mat close to the liquid-air interface in flasks. For flask growth, a standardized *A. fumigatus* suspension was inoculated into 500 ml polystyrene tissue-culture flasks containing 100 ml of RPMI-1640 medium (final concentration 10^5 conidia/ml) and incubated at 30 °C for 96 h. Biofilms on disks were formed by using a modified in vitro model, described previously (Ferreira et al., 2009, 2015). To form *A. fumigatus* biofilms, sterile polystyrene disks (Biosurface Technologies, Bozeman, MT) were placed in 12-well tissue culture plates (Corning Inc., MD, NY). Each well contained 3 ml of fresh RPMI-1640 medium (Lonza, Walkersville, MD) with 10^5 conidia/ml. Disks were incubated at 37 °C for 16 h with shaking at 70 rpm, to allow the fungal cells to attach. Following the attachment phase, disks were gently rinsed in sterile saline (Baxter Healthcare Corp., Cambridge, MA), transferred to new plates containing fresh RPMI-1640 medium, and incubated for an additional 24 h at 37 °C with shaking at 70 rpm.

2.1. SEM processing

Disks and biofilm mats were harvested and washed in situ twice with 100 ml of phosphate-buffered saline (PBS) to remove planktonic cells. Samples were fixed in 4% paraformaldehyde (PFA) with 2% glutaraldehyde (GA) in 0.1 M sodium cacodylate buffer for varying incubation times (45 min–24 h, see Table 1). Samples were then briefly rinsed in the same buffer before post-staining with 1% OsO_4 for incubation times of 0 to 45 min (Table 1). For conventional SEM, OsO_4 -treated samples were rinsed in water and gradually dehydrated in increasing concentrations of ethanol (50, 70, 90, 100%, 5 min each). Samples were then either dried with HMDS, or critically point dried with liquid CO_2 using a Tousimis Autosamdri 815A and 15 min purge time (Tousimis, Rockville, MD). Dried samples were sputter-coated (50 Å, Au/Pd) before imaging with a Hitachi 3400N SEM operated at 10 kV under high vacuum, using an Everhart-Thornley (ET) Secondary Electron (SE) detector, and a Zeiss Sigma FESEM using InLens SE detection at 2 kV (Carl Zeiss Microscopy Inc., Thornwood, NY).

2.2. VP-SEM application

Hydrated samples were visualized fully hydrated and either unfixed, or fixed in aldehydes as described above for conventional SEM, followed by post-fixation (45 min) in aqueous OsO_4 to enhance contrast of cellular material. Samples were mounted in water on 10 mm cup-shaped

Table 1
Summary of fixation and drying parameters used to process *A. fumigatus* biofilms for SEM visualization.

Biofilm culture (×2): flask versus disk							
2%GA + 4%PFA, postfix 1% OsO_4				2%GA + 4% PFA (no OsO_4)			
24 h fix		45 min fix		24 h fix		45 min fix	
CPD	HMDS	CPD	HMDS	CPD	HMDS	CPD	HMDS
Hydrated: VP-SEM (60 Pa)				Hydrated: VP-SEM (60 Pa)			

stubs custom-fitted for the Deben cold-stage (Deben Ltd., Suffolk, UK), and temperature was gradually decreased during evacuation, following a correlated graph for sublimation temperature and pressure of water. VP-SEM was carried out with a Hitachi S-3400N VP-SEM (Hitachi High Technologies, Pleasanton, CA) operated at 15 kV and 50–60 Pa, using Backscattered Electron (BSE) detection and cold-stage (−25 °C) control of hydration.

2.3. Staining with Ruthenium Red

Disk grown *A. fumigatus* biofilms were fixed in 4% PFA with 2% GA for 45 min (see Section 2.1) and rinsed in buffer (2 × 5 min), before (i) post-fixation in 0.01% Ruthenium Red for 1 h, or alternatively, (ii) post-fixation in 0.01% Ruthenium Red (1 h) followed by incubation in OsO_4 (45 min). Samples were rinsed in water (3 × 5 min) after incubation in each metal solution, and visualized fully hydrated using VP-SEM as described above (Section 2.1). Samples were kept in water at 4 °C for a maximum of 24 h before imaging.

2.4. Staining with Ruthenium tetroxide (RuO_4)

Disk grown *A. fumigatus* biofilms were fixed in 4% PFA with 2% GA for 45 min (see Section 2.1) and rinsed in buffer (2 × 5 min), before post-fixation in 0.5% RuO_4 (1 h). All residual RuO_4 was removed by repeated rinsing (3 × 5 min) in water, before visualizing biofilms fully hydrated using VP-SEM as described above (Section 2.1). Samples that were not visualized directly after staining were kept in water at 4 °C and imaged within 24 h.

2.5. Ionic Liquid (IL) treatment

Pellicles of flask grown *A. fumigatus* biofilms were fixed as before in 4% PFA with 2% GA, rinsed in 0.1 M Na cacodylate buffer (1 × 5min) and, after removing most residual liquid, submerged in 100 μl of either 5%, 10% or 20% HILEM™ Ionic Liquid (Hitachi High Technologies, Pleasanton, CA) for 1 h at ambient temperature. Samples were removed from IL and left to dry overnight on filter paper in a desiccator before mounting and imaging (without Au/Pd sputter-coating) with a Hitachi 3400N SEM operated at 5 and 10 kV under high vacuum, using SE detection. Based on the results obtained with *A. fumigatus* pellicles, disk grown *A. fumigatus* biofilms were submerged in 10% IL (1 h) and dried and mounted similarly before SEM imaging under high vacuum and without further conductive (Au/Pd) coating.

2.6. Cryofixation

Disk grown *A. fumigatus* biofilms were cryoprotected with 10% glycerol for 2 h at 4 °C, plunge-frozen in liquid nitrogen and lyophilized before mounting and Au/Pd sputter-coating for FESEM observation as described above (see Section 2.1).

3. Results and discussion

A. fumigatus biofilms form as a spongy mass of hyphae when grown at the liquid-air interface in a glass flask. When cultured on a plastic disk submerged in liquid, the biofilm is a matted network of hyphae closely associated with the solid substrate. The impact of various experimental parameters (see Sections 2.1–2.6) on biofilm structure is discussed below.

3.1. SEM modality

3.1.1. VP-SEM (Fig. 1)

Inherent to VP-SEM is the poor SNR (Signal to Noise Ratio) due to gas and moisture in the specimen chamber, and the ability of water to serve as an electron dense sheet which may coat individual cells (hyphae) and obscure fine cellular features. However, VP-SEM is ideally suited to visualize the native 3D architecture of hydrated biofilms, which often collapses during dehydration for conventional SEM. It does not typically employ drying and sputter-coating for conductivity and, thus, also enables more rapid analysis. Stabilization of cells with aldehyde fixatives generally improved structural preservation (Fig. 1), while post-fixation with OsO_4 (and other heavy metals, see Section 3.3) enhanced the BSE signal (Fig. 1), which is the detector of choice for this EM modality (in Hitachi S-3400N). Additionally, the lipid-binding properties of OsO_4 highlighted intra and extracellular lipids (often as droplets) in the fungal mycelium (Fig. 1 arrows). Therefore, using VP-SEM instead of high-vacuum SEM may better reveal hydrated 3D architecture, but limits ultrastructural analysis of individual cells and ECM.

3.1.2. SEM and FESEM (Figs. 2 & 3)

In our SEM analysis, a conventional Everhart-Thornley (ET)-SE detector was used, whereas our FESEM investigation applied an InLens SE detector. In both cultures (flask and disk grown), fungal hyphae occurred as flat filamentous structures, which were frequently connected with ECM material. ECM occurred either as stretched sheets (Figs. 2B & 3, white arrows) or fine, often reticulated fibers (Figs. 2B & 3, yellow arrows). Using high resolution FESEM, ECM was additionally characterized as an apparent rough, granular or vesicular coating (Fig. 3, red arrows) closely associated with hyphae. The nature of similar vesicles was suggested by our recent Transmission EM (TEM) analysis combined with solid-state NMR, which revealed isolated ECM from *A. fumigatus* to be vesicular as well as fibrous in nature (Reichhardt et al., 2015). Fungal biofilms, which apparently lacked ECM by gross inspection, thus revealed surprising quantities of ECM with high-efficiency InLens SE detection, which obtains high lateral resolution and edge contrast at low accelerating voltages. Post-fixation with OsO_4 generally enhanced SE and BSE detection in both SEM and FESEM analyses. Shorter periods in aldehyde fixatives resulted in improved separation of fine structural features (Figs. 2 & 3), while longer fixation times caused a collapse of fungal mycelium and ECM fibers.

3.2. Processing for conventional (high-vacuum) SEM

3.2.1. Primary fixation

The high protein content of ECM, as reported by Reichhardt et al. (2015), results in efficient ultrastructural preservation of ECM by aldehydes. Primary fixation with aldehydes has been proven to provide the optimal ultrastructural preservation of living cells, in addition to preventing disruption during further processing steps (Bozzola and Russell, 1999). While GA provides superior stabilization of structure through its terminal aldehyde groups that crosslink amino groups in proteins, PFA has been included in low concentrations (up to 4%) to penetrate and preserve living cells more rapidly than the larger GA molecule (Karnovsky, 1965). By introducing this combination of PFA with GA, both rapid and more efficient stabilization of proteins is therefore accomplished. Since protein is a universal constituent of cells, and has also been found to be a major component of the ECM of *A. fumigatus* biofilms (Reichhardt et al., 2015), primary fixation with aldehydes (PFA and GA) stabilizes both the cellular and extracellular components of *A. fumigatus* biofilms. One can envision that aldehyde fixation crosslinks soluble proteins to each other and to fixed membranes and the cytoskeleton, as well as extracellular components in these biofilms. Its specificity is not limited to proteins, and GA may also react with lipids, nucleic acids and carbohydrates. Since the optimal concentration of primary fixatives that would accomplish denaturation of proteins, without additional artifacts of autolysis and extraction by different tonicities, has been proven to be below 4% PFA and 2–3% GA (Bozolla and Russell, 1999; Dykstra, 1992; Coetzee and Van der Merwe, 1984, 1986; Bone and Denton, 1971; Anniko and Lundquist, 1977), we used similar concentrations of aldehydes for preservation of *A. fumigatus* biofilms. However, while extended incubation times in aldehydes are a generally

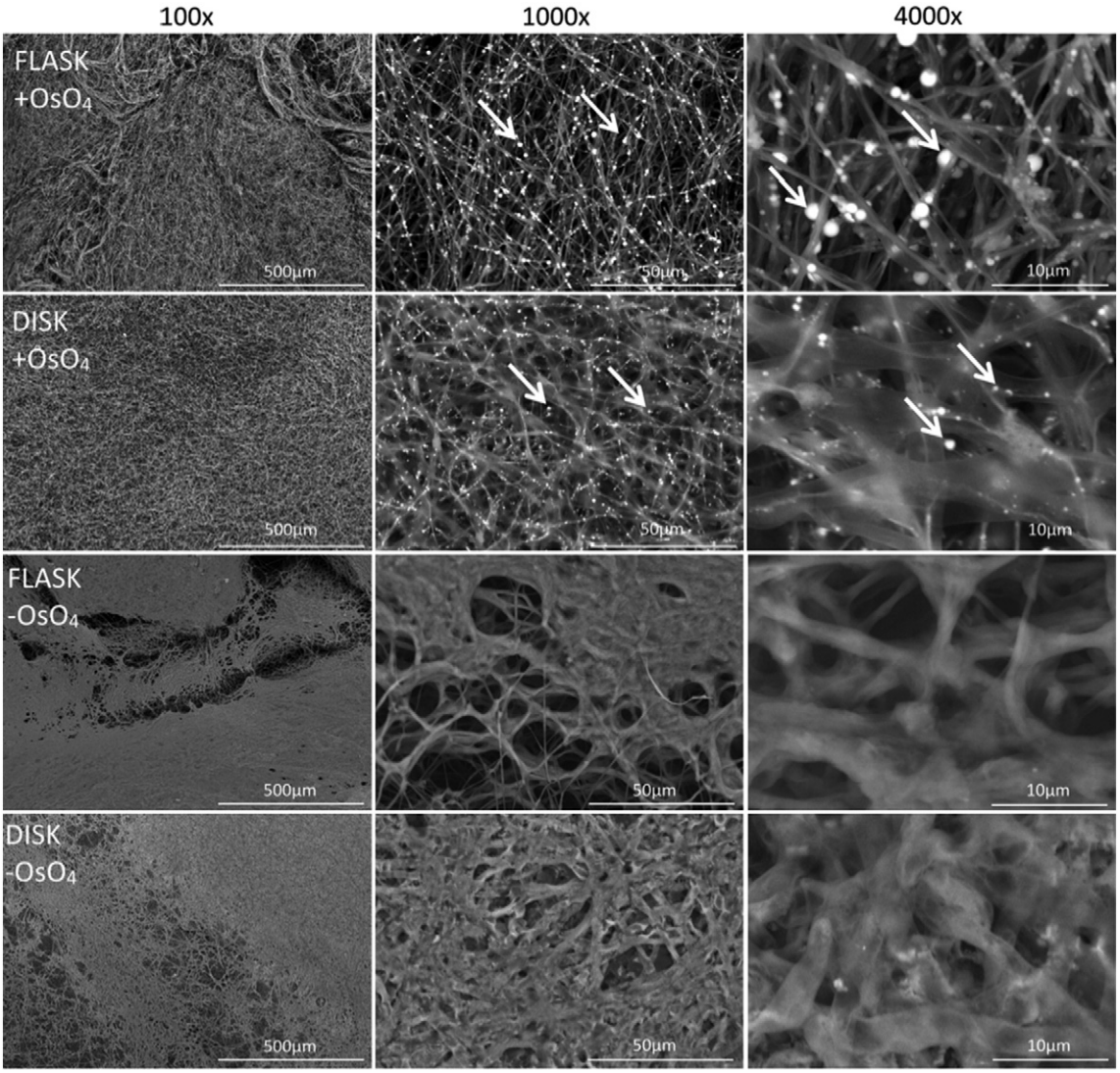

Fig. 1. Flask vs. disk-grown: VP-SEM of hydrated and unfixed *A. fumigatus* biofilms including OsO_4 (two upper rows) and excluding OsO_4 (two lower rows) post-fixation. OsO_4-enhanced lipids are indicated by arrows.

accepted laboratory practice, in the case of *A. fumigatus* biofilms, prolonged fixation (≥24 h) often led to a collapse of fine features (Fig. 2A-columns A, B) and a denser appearance of biofilm structure, probably due to increased binding of associated and complex matrix materials, and physico-chemical factors in a hydrated environment. By limiting the incubation time in primary fixatives to less than an hour (45 min in this study) we found improved preservation of ECM ultrastructure – which was the primary objective of our SEM investigations. This supports the observation of Bozzolla and Russell (1999) that, due to the introduction of artifacts during fixation, one always selects a particular fixation protocol for 'its ability to preserve one ultrastuctural feature over another'.

3.2.2. Secondary fixation

OsO_4 is generally used as secondary fixative, both to stabilize especially the lipid moieties of cells, and to act as 'stain' (contrasting agent) in being a high molecular weight reagent. Its penetration rate is slower than that of GA, but since exposure for longer than 1.5 h can lead to extraction of materials (Bozzola and Russell, 1999), we similarly used short (<1 h) fixation times in OsO_4. In the case *A. fumigatus* biofilms, post-fixation with OsO_4 generally improved ultrastructural preservation, while enhancing SNR for both SE and BSE detection. The improved signal from heavy metal staining also resulted in increased brightness and contrast in *A. fumigatus* biofilms, which enabled improved characterization of cellular versus extracellular biofilm components (Fig. 2B upper row, arrows). Since the phospholipid component of cellular membranes, as well as the lipid component of ECM were better preserved with addition of OsO_4, biofilm components also appeared less aggregated after post-fixation with OsO_4 (Fig. 2A, rows 1 & 2).

3.2.3. CPD versus HMDS

CPD improved ultrastructural preservation of fine features, notably in ECM, while final drying with HMDS often caused aggregation of hyphae and fine structures. A. fumigatus biofilms that were dried with HMDS often appeared as aggregated hyphae connected by sheets of ECM lacking fibrous ultrastructural features, and with collapsed vesicles. This comparison illustrates the influence different drying methods can have on analysis. HMDS provides a rapid low-cost alternative to CPD where sample format (or space and funding) limits the use of CPD. However, results with *A. fumigatus* biofilms are superior with CPD. CPD is designed to avoid perturbations from the surface tension of a decreasing meniscus resulting from the evaporating dehydrating liquid by moving the intermediary liquid (liquid CO_2) to its critical point (where the densities of liquid and gas are identical) at which point the residual gas can be removed. Thus, the effect on final structure should be

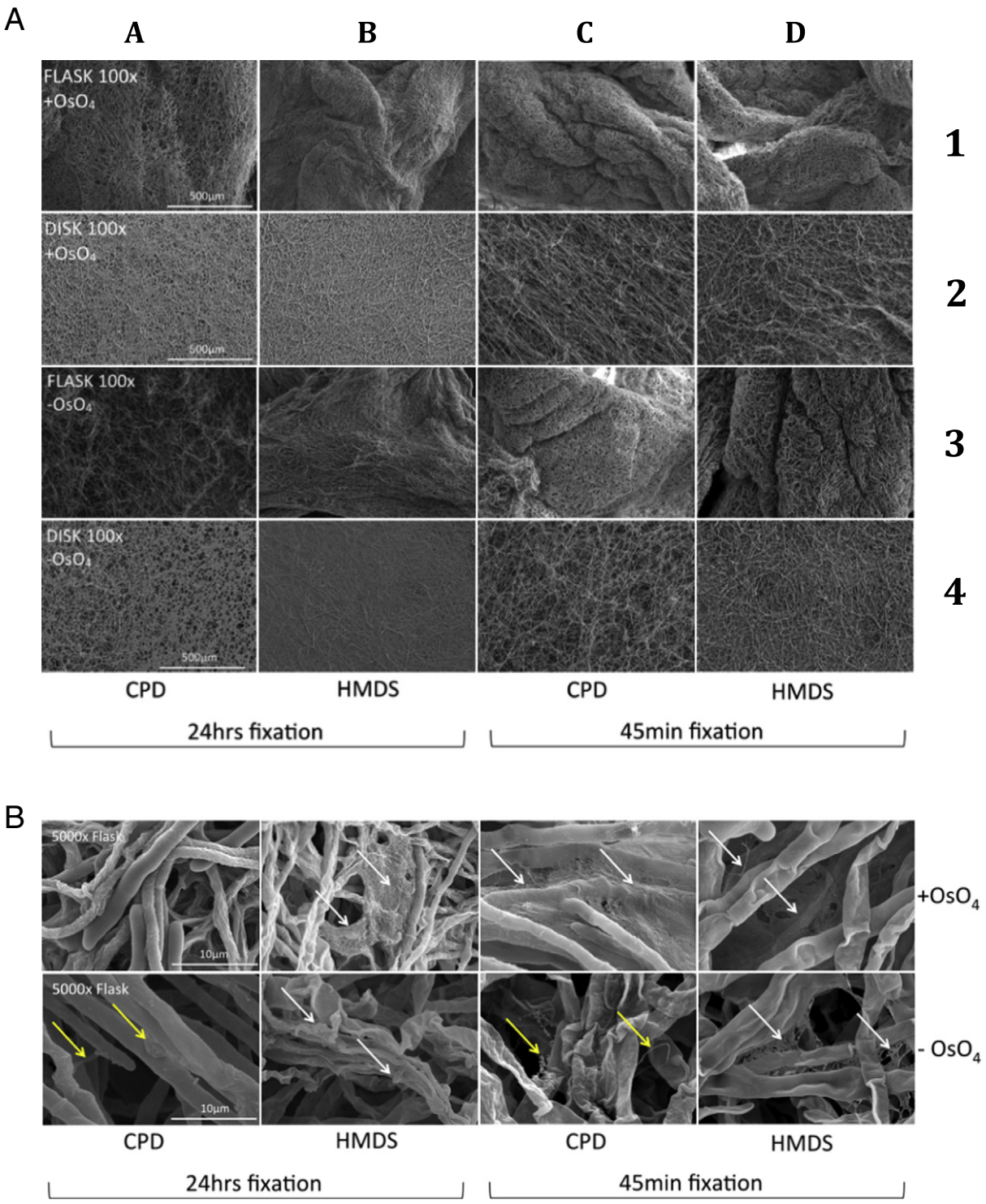

Fig. 2. A: Flask vs. disk-grown *A. fumigatus* biofilms, CPD vs. HMDS dried, 24 h vs. 45 min fixation, with OsO_4 (upper rows) and without OsO_4 (lower rows). Prolonged fixation (columns A & B) results in denser appearance of biofilm through collapsed fine features. Addition of OsO_4 similarly led to less aggregated biofilm architecture (rows 1 & 2). A combination of OsO_4 and CPD treatment therefore resulted in optimal biofilm structure (C2: column C, row 2). B: High magnification (5000×) micrographs of flask-grown *A. fumigatus* biofilms illustrating hyphal and ECM features: CPD vs. HMDS dried; 24 h vs. 45 min fixation; $\pm OsO_4$. Post-fixation with OsO_4 led to improved SNR and contrast-enhanced resolution of cellular and extracellular biofilm components. White arrows: ECM occurred as stretched sheets. Yellow arrows: ECM occurring as fine or reticulated fiber.

carefully evaluated to determine drying–associated artifacts. At lower magnification, this effect was most obvious in disk-grown biofilms (Fig. 2A). At higher magnification, drying artifacts were evident in ECM from both disk and flask grown cultures. The effect is exacerbated when OsO_4 was excluded during fixation (Fig. 2B).

3.2.4. Disk grown biofilms versus flask grown pellicles

Disk grown biofilms formed a flatter, two-dimensional architecture than the spongy three-dimensional structure of flask grown pellicles. Pellicles exhibited large pores and channels surrounding an elaborate network of intertwined hyphae, which were often partially compressed.

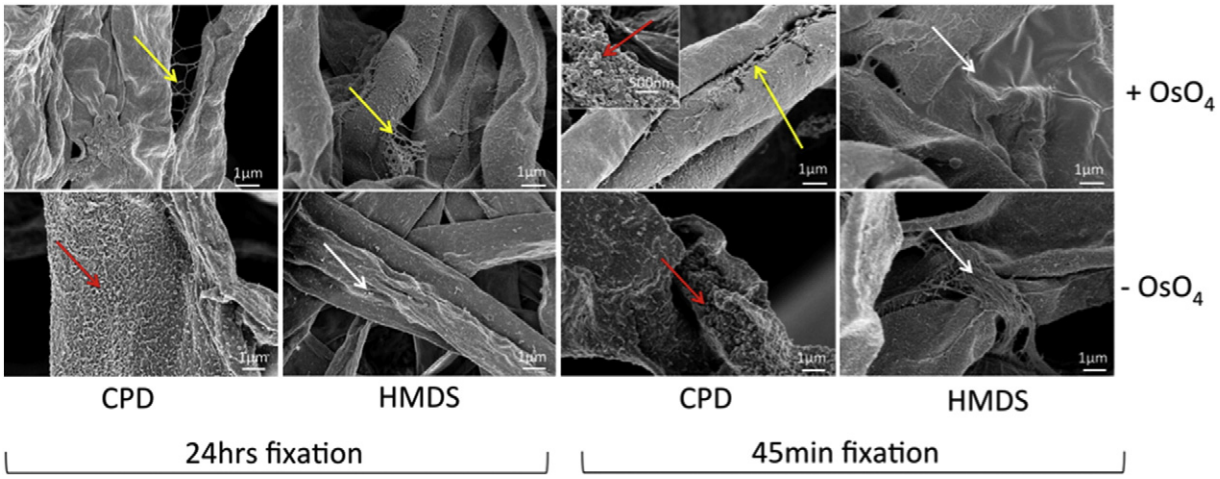

Fig. 3. FESEM of *A. fumigatus* biofilms, with and without OsO_4 post-fixation. ECM features are characterized with high definition InLens SE detection at 10,000× magnification. White arrows = stretched sheet of ECM; yellow arrows = fine or reticulate fibers of ECM; red arrows = ECM occurring as a rough, granular or vesicular coating, closely associated with hyphae. Inset shows ECM as a vesicular coating at 20,000× magnification.

This apparent vacuolization of hyphae may result from aging or stress factors in the deeper biofilm layers (Lin and Austriaco, 2014, Flemming et al., 2016). Hyphae on disks were closely associated with the plastic substrate, often extended in parallel growth-patterns, and revealed more spherical ECM vesicles than in the pellicles, where ECM was mostly visible as a network of fibrous material forming fine sheets that stretch between hyphae. The appearance of ECM largely depended on the fixation and drying techniques (Sections 3.2.1–3.2.3)

3.2.5. Fixation time with aldehydes

Fixing for prolonged times (at least 24 h), as typically done with biological samples, caused a collapse of ECM and hyphae, resulting in poor preservation of biofilm architecture, loss of 3D structure attributed to water loss through dehydration techniques. Fixation for shortened times (<1 h) resulted in excellent preservation of both cellular and extracellular components, and thereby improved interpretation of ultrastructural features, i.e. mycelium/hyphae, ECM fibers and vesicles. For *A. fumigatus* biofilms, such shortened fixation and post-fixation conditions proved to be optimal for relevant interpretation of both hyphae and ECM ultrastructure (Fig. 2A, B & Fig. 3).

3.2.6. Cryofixation

Biofilms that were cryo-protected and prepared by plunge-freezing in liquid N_2, followed by lyophilization, showed remarkable preservation of both cellular (hyphae) and ECM ultrastructure. Hyphae remained separated and non-compacted, while ECM was present as fine reticulate fibers (Fig. 4). This technique requires minimal preparation, while preliminary fixation with PFA and GA may also be included. Villena et al. (2010) similarly observed differences in *Aspergillus niger* biofilm morphology when applying cryo-fixation techniques to biofilms grown as pellicles versus substrate (cloth)-attached films.

3.2.7. Ionic Liquid treatment

Ionic Liquids are salts that exist in liquid state at room temperature and do not evaporate under vacuum conditions in EM applications (Arimoto et al., 2008; Asahi et al., 2015.). It provides both electrical conductivity and hydration to biological specimens, and thereby enables electron microscopic visualization of specimens without dehydration or sputter-coating with a conductive metal. *A. fumigatus* pellicles (Fig. 5A) and disk grown biofilms (Fig. 5B) showed remarkable conductivity and contrast, while retaining overall biofilm structure, when treated with HILEM™ Ionic Liquid. Fixation with aldehydes may be included

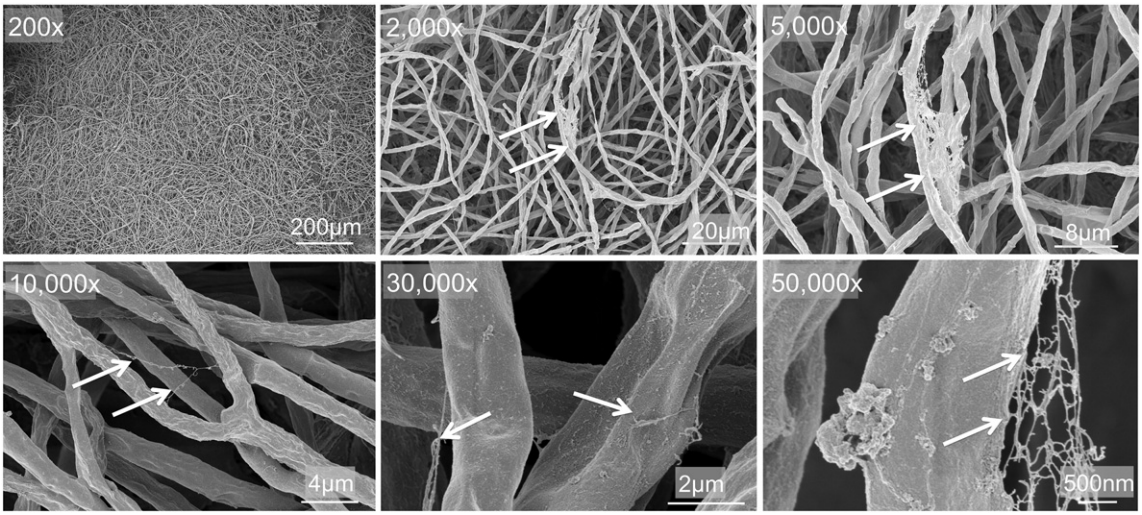

Fig. 4. Cryofixation of disk grown *A. fumigatus* biofilms reveals well-preserved hyphae and ECM (arrows) in a non-collapsed 3D biofilm architecture.

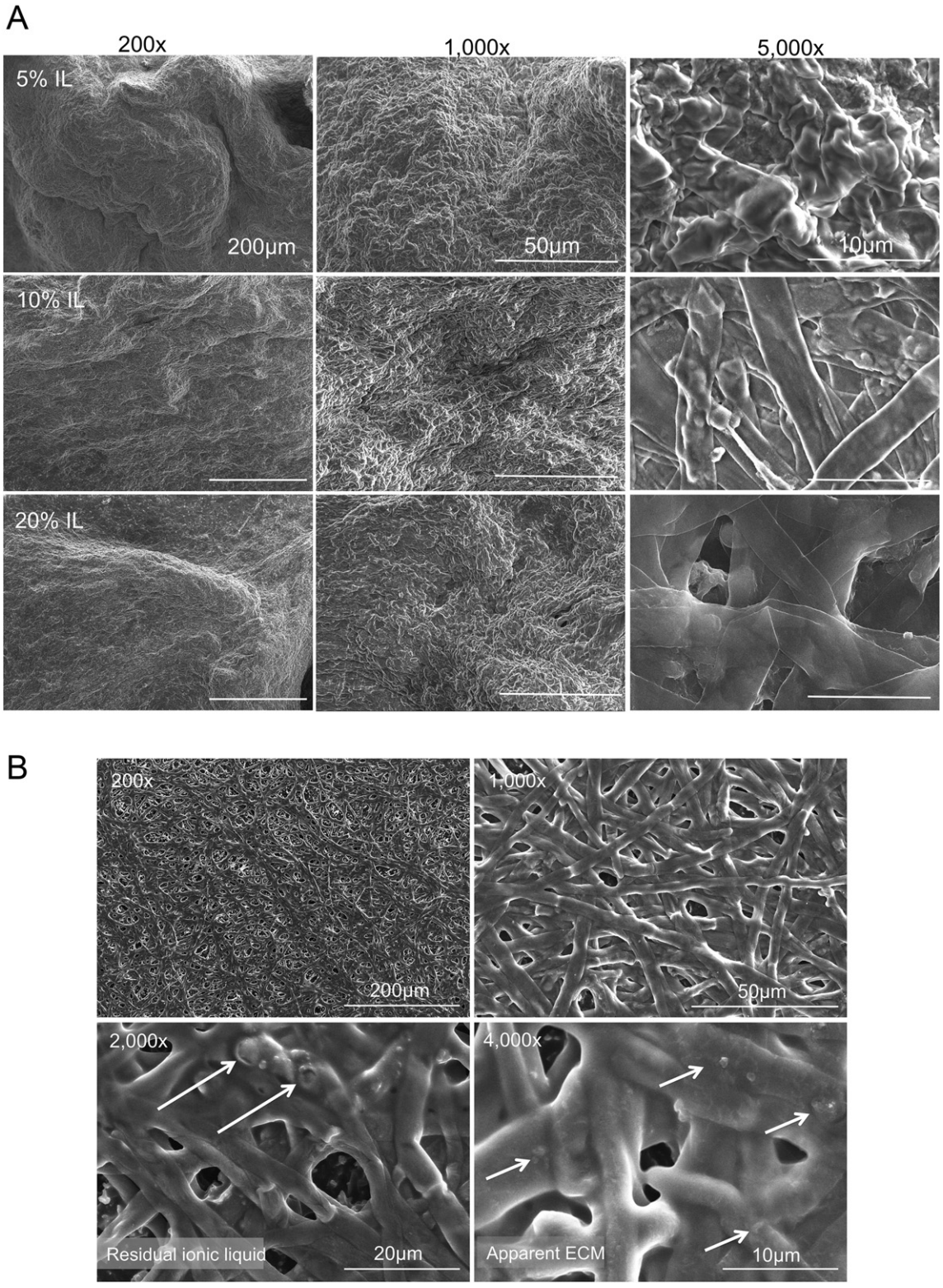

Fig. 5. A: *A. fumigatus* biofilm pellicles treated with 5%, 10% and 20% HILEM Ionic Liquid, and imaged at increasing magnification (200×, 1000×, 5000×) at 5 kV, using ET-SE detection and without Au/Pd sputter-coating. Lower concentrations (5%) of IL exhibited more artifacts of beam interference, while biofilm topography, and associated charging artifacts, played a more important role than IL concentration in final image quality and resolution. B: Disk grown *A. fumigatus* biofilms treated with 10% HILEM Ionic Liquid, and imaged at increasing magnification (200×, 1000×, 2000× and 5000×) at 5 kV, using ET-SE detection and without Au/Pd sputter-coating. Hydrated biofilm architecture was retained, while fine features were often hidden by residual IL (2000: arrows). After thorough draining of IL, apparent ECM could still be observed at higher magnification (4000×: arrows).

to stabilize fine features, though was not a prerequisite to visualize biofilm structure, and did not enhance image quality (Joubert and McDonald, 2016). Since *A. fumigatus* biofilms were hydrated when treated with Ionic Liquids, the natural biofilm architecture was retained. This was especially obvious at lower magnification (Fig. 5A & B: 200× and 1000×), while at higher magnification hyphae appeared aggregated and closely associated, mostly due to water and IL filling pores and channels between hyphae (Fig. 5A & B: 2000–5000×). Fibrous ECM

was not observed, since such fine structures will only be revealed after extraction of water, as in conventional SEM. Residual IL may limit resolution of fine surface features (Fig. 5B arrows), and at high magnification may result in artifacts such as small bubbles appearing under the electron beam (data not shown). Biofilm topography influenced sample conductivity, and this was observed especially where the biofilm was forming a convoluted 3D structure that was lifted away from the substrate during drying. Using lower accelerating voltages provided a suitable solution, though while at the same time limiting resolution at higher magnification, which can only be attained at higher accelerating voltages. Treating *A. fumigatus* pellicles with an increasing series of IL concentrations (Fig. 5A), suggested 10% IL to be an optimal concentration to enhance conductivity, limit charging artifacts, and prevent accumulation of IL in porous areas. In the subsequent treatment of disk grown *A. fumigatus* biofilms (Fig. 5B), only 10% IL was used, and samples imaged at high vacuum without sputter-coating, and using ET-SE detection. Draining off all residual IL is important where either porous areas or fine features need to be resolved. Given the rapid preparation, needing very few materials and no ancillary equipment, IL provides a valuable tool to explore biofilms in their natural (hydrated) state under high vacuum and using SE detection (Sakaue et al., 2014; Joubert and McDonald, 2016).

3.3. Contrasting for VP-SEM (Figs. 1 & 6)

Since VP-SEM systems mostly use BSE detection for visualization, with the signal consequently related to the atomic weight of the specimen, inclusion of heavy metals during processing can provide both a stabilization (fixation) aspect in addition to improving contrast and resolution. OsO_4 has been proven throughout the history of EM to provide excellent fixation in cells (Porter and Kallman, 1953). It oxidizes double bonds in unsaturated fatty acids and is reduced to an electron-dense product at the reduction site (Bozzola and Russell, 1999). Contrasting with OsO_4 therefore provides a specific contrasting agent for lipid-containing areas in the cell, though it has been described (Porter and Kallmann, Bozzola and Russell) to react with various other cell components, including proteins – and also acts as a mordant, in later combining with stains and contrasting agents. Here we observed enhanced contrasting of lipid droplets inside hyphae, in addition to improved resolution of cell membranes and biofilm structure (Figs. 1 & 6).

Ruthenium Red has similarly been used over decades (Reimann, 1961; Dierichs, 1979; Luft, 1971) as a cell wall stain in electron microscopy, and not only binds with phospholipid membranes, but also associates with Ca^{2+}-binding proteins. Both specific and non-specific adsorption models have been proposed (Voelker and Smejtek, 1996). Chemical reactions between Ruthenium Red and OsO_4 also apparently bind these heavy metals to cell surfaces, where it provides contrast enhancement (Dierichs, 1979). We applied Ruthenium Red both as single reagent, and in combination with OsO_4 (see Section 2.3). As a single stain, contrast was enhanced in hyphae as well as ECM (Fig. 6 top row, short arrows), probably due to the ability of Ruthenium Red to bind to both lipid and protein components of the cellular and extracellular biofilm components. In combination with OsO_4, the lipid component of hyphae was more strongly enhanced, similar to staining with OsO_4 alone (Fig. 6, second row, long arrows). Both forms of Ruthenium Red (with and without OsO_4) provide a valuable contrasting alternative to biofilms, and since Ruthenium Red is much less toxic than OsO_4, this reagent can be used with great success in VP-SEM applications.

We finally applied RuO_4 as contrasting reagent in hydrated and aldehyde-fixed *A. fumigatus* biofilms. RuO_4 is closely related to OsO_4, fixes membranes and polymeric materials, and has been described as a 'far more vigorous' oxidant than OsO_4 (Trent et al., 1983). According to Gaylarde and Sarkany (1968) RuO_4 also reacts more strongly with more polar lipids, as well as proteins, glycogen and monosaccharides.

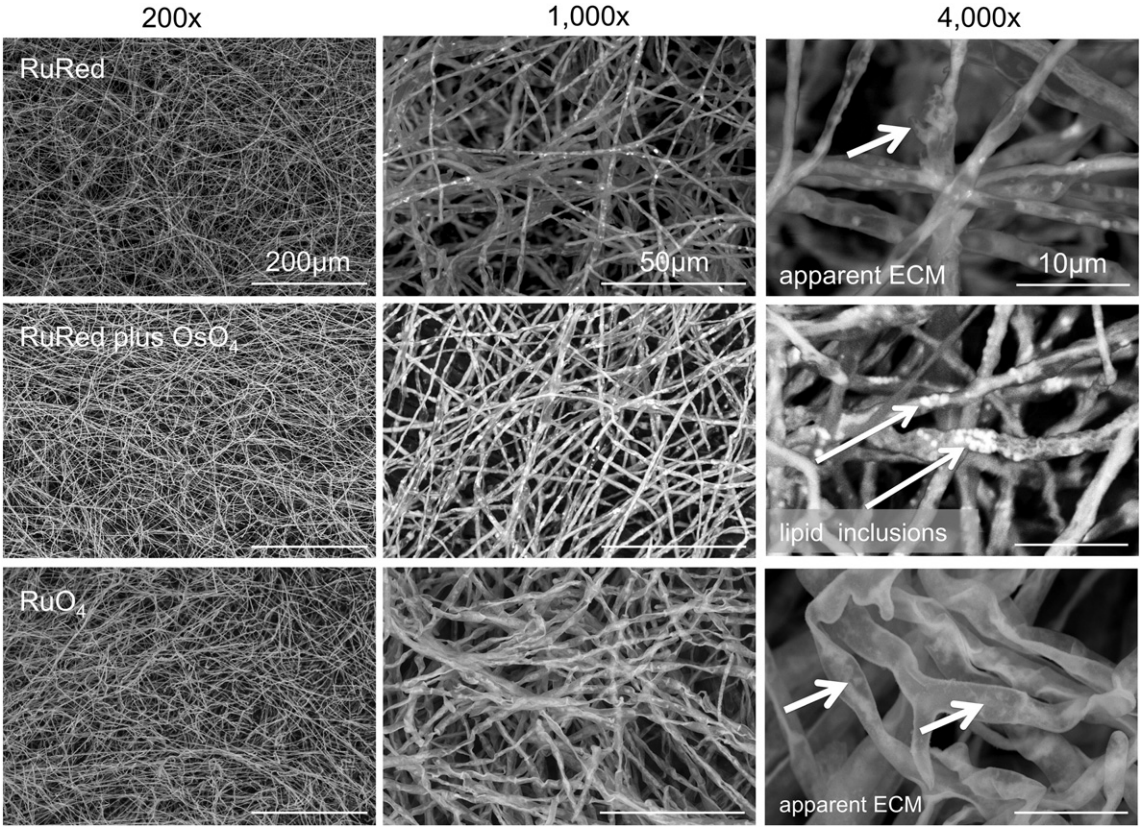

Fig. 6. VP-SEM of fully hydrated disk grown *A. fumigatus* biofilms after post-fixation with various heavy metals shows enhanced contrasting of hyphae, ECM (short arrows) and included lipids (long arrows). Ruthenium Red (top row) and RuO_4 (third row) show improved fixation and resolution of ECM, while addition of OsO_4 (second row) highlights lipid inclusions over ECM features.

Our results with VP-SEM visualization of *A. fumigatus* biofilms illustrated this heavy-metal reagent as an excellent contrasting agent for both cellular and ECM components of the biofilm (Fig. 6, third row). Hyphae were well preserved, while resolution was enhanced by the gain in contrast. ECM showed similar enhanced contrast, and the fibrous ultrastructure was resolved both on and between hyphae (Fig. 6 short arrows) - an aspect that was unattainable when OsO_4 was included as contrasting agent. Given the protein and lipid moieties of *A. fumigatus* biofilms (Reichhardt et al., 2015) we introduce this heavy-metal reagent as a valuable fixative and contrasting agent in fungal biofilm studies.

Our results suggest that consistent high-resolution ultrastructural SEM analysis of cellular features and ECM of *A. fumigatus* biofilms can be achieved using a relatively short fixation time and including OsO_4 post-fixation, followed by CPD. It is also evident, even at low magnifications, (Fig. 2A) that the combination of extended fixation times, a lack of OsO_4 combined, and HMDS drying yield the poorest preservation of ultrastructure in both disk and flask cultures.

In Table 2 we compare the described processing techniques to suggest a practical workflow in the laboratory, and highlight the time, equipment and expertise needed for each procedure.

4. Conclusions

In-depth analysis of compositional, structural and functional aspects of *A. fumigatus* is needed to identify new antifungal targets (Kaur and Singh, 2014) and can ultimately be leveraged to design therapeutic agents for the control of *A. fumigatus* biofilm-associated infection and contamination. Electron microscopy is unparalleled in its ability to visualize microbial biofilms. This visualization is crucial in connecting differences in biofilm composition with function. However, variations in sample preparation protocols, microscope selection, and acquisition parameters can influence the observed ultrastructure in biological samples, particularly biofilms.

From the broadest perspective, VP-SEM is a superb modality where hydrated 3D biofilm structure is of greater importance than ultrastructural surface features of individual cells (hyphae in *A. fumigatus*). However, water is electron dense. Trapped water in hydrated biofilms can cause closely associated hyphae to appear as thick strands, limiting resolution and even preventing distinction between hyphal strands and ECM. Thus, where ultrastructural features of cellular and ECM components are desired, high-resolution SEM and FESEM techniques using SE detection are superior.

For each imaging modality (VP-SEM with BSE detection, conventional SEM with ET-SE detection, and FESEM with InLens SE detection), we observed that the maintenance of biofilm ultrastructure during SEM analysis also depended on the sample fixation parameters (fixative and fixing time) and sample drying method (CPD vs. HDMS). Optimal parameters also differed for pellicles (with biofilms formed at the air-liquid interface) and biofilms attached to plastic. Thus, sample preparation parameters should be optimized for any new biofilm sample. Our general recommendations for SEM visualization of *A. fumigatus* biofilms include the following: (1) A short primary fixation time of up to 1 h is ideal for sample preparation, where longer fixing times, e.g. 24 h, compromise the integrity of the biofilm architecture. (2) Post-fixation with OsO_4 yields improved contrast and visualization of cellular versus extracellular regions, attributed to the enhanced staining of lipids within cells and as extracellular component of ECM. Due to the complex and varying nature of ECM, other heavy-metal reagents such as Ruthenium Red and RuO_4 may provide both a wider spectrum and more specific contrasting of biofilm components. (3) Sample drying using CPD is superior to HDMS and improves the ultrastructural preservation of fine features in the ECM. (4) Specimen preparation with cryo-fixation and lyophilization provides a valuable and rapid alternative to conventional chemical fixation and drying. In summary, our analysis presented here emphasizes the complexities in visualizing the attached lifestyle of microbial communities and provides our results and recommendations for visualizing biofilms formed by *A. fumigatus*.

Table 2
Comparison of processing techniques, protocols and equipment for SEM/FESEM and VP-SEM.

	Conventional SEM	VP-SEM	Ionic Liquid	Cryo-fixation
Primary fix	45 min	Optional	Optional	Plunge-LN_2
Rinse	3 × 5 min		Immersion IL [1 h]	–
Secondary fix/contrast	45 min	30–60 min	–	–
Rinse	3 × 5 min	3 × 5 min	–	–
Dehydrate	Increasing ethanol series [1 h]	–	–	–
Drying (CPD)	CPD [1 h] HMDS [1 − 12 h]	–	Air/vacuum dry [1–12 h]	Lyophilize [1 h]
Mounting	Yes [15 min]	In SEM chamber	Yes [15 min]	Yes [15 min]
Sputter-coating	Yes [15 min]	–	–	Yes [15 min]
Equipment	Fume hood, CPD, sputter coater	Fume hood	–	Freeze-dryer
Expertise	High	Medium	Low	Medium
Resolution	SE: high	BSE: low	SE: medium	SE: high
Total time	4.5 h (min)	0.75 h	2.25 h (min)	1.5 h

Acknowledgements

These studies were partially supported (D.A.S.) by a grant from the Child Health Research Institute, Stanford Transdisciplinary Initiatives Program, and a gift from John Flatley. L-M.J. was partially supported by the Beckman Foundation and a Technology Innovation mini-grant and J.A.F. by a grant from the Brazilian National Council for Scientific and Technological Development (CNPq). The material is based in part upon work supported (L.C.) by the National Science Foundation CAREER Award (1453247). Hitachi High Technologies is thanked for providing HILEM™ IL. Kent McDonald is gratefully acknowledged for fruitful discussions.

References

Alhede, M., Qvortrup, K., Liebrechts, R., Høiby, N., Givskov, M., Bjarnsholt, T., 2012. Combination of microscopic techniques reveals a comprehensive visual impression of biofilm structure and composition. FEMS Immunol. Med. Microbiol. 65, 335–342.

Anniko, M., Lundquist, P.-G., 1977. The influence of different fixatives and osmolality on the ultrastructure of the cochlear neuroepithelium. Arch. Otorhinolaryngol. 218: 67–78. http://dx.doi.org/10.1007/BF00469735.

Arimoto, A., Sugimura, M., Kageyama, H., Torimoto, T., Kuwabata, S., 2008. Development of new techniques for scanning electron microscope observation using ionic liquid. Electrochim. Acta 53 (21):6228–6234. http://dx.doi.org/10.1016/j.electacta.2008.01.001.

Asahi, Y., Muira, J., Tsuda, T., et al., 2015. Simple observation of *Streptococcus mutans* biofilm by scanning electron microscopy using ionic liquids. AMB Express 5 (1), 6–14.

Beauvais, A., Schmidt, C., Guadagnini, S., Roux, P., Perret, E., Henry, C., Paris, S., Mallet, A., Prevost, M.C., Latge, J.P., 2007. An extracellular matrix glues together the aerial-grown hyphae of *Aspergillus fumigatus*. Cell. Microbiol. 9:1588–1600. http://dx.doi.org/10.1111/j.1462-5822.2007.00895.x.

Beauvais, A., Loussert, C., Prevost, M.C., Verstrepen, K., Latge, J.P., 2009. Characterization of a biofilm-like extracellular matrix in FLO1-expressing *Saccharomyces cerevisiae* cells. FEMS Yeast Res. 9:411–419. http://dx.doi.org/10.1111/j.1567-1364.2009.00482.x.

Beauvais, A., Fontaine, T., Aimanianda, V., Latge, J.P., 2014. *Aspergillus* cell wall and biofilm. Mycopathologia 178:371–377. http://dx.doi.org/10.1007/s11046-014-9766-0.

Bone, Q., Denton, E.J., 1971. The osmotic effects of electron microscope fixatives. J. Cell Biol. 49 (3):571–574. http://dx.doi.org/10.1083/jcb.49.3.571.

Bozzola, J.J., Russell, L.D., 1999. Electron Microscopy Principles and Techniques for Biologists. second ed. Jones and Bartlett Publishers, Sudbury, MA.

Bray, D.F., Bagu, J., Koegler, P., 1993. Comparison of hexamethyldisilazane (HMDS), Peldri II, and critical-point drying methods for scanning electron microscopy of biological specimens. Microsc. Res. Tech. 26, 489–495.

Cegelski, L., 2015. Bottom-up and top-down solid-state NMR approaches for bacterial biofilm matrix composition. J. Magn. Reson. 253:91–97. http://dx.doi.org/10.1016/j.jmr.2015.01.014.

Chotirmall, S.H., Mirkovic, B., Lavelle, G.M., McElvaney, N.G., 2014. Immunoevasive *Aspergillus* virulence factors. Mycopathologia 178, 363–370.

Coetzee, J., Van der Merwe, C.F., 1984. Extraction of substances during glutaraldehyde fixation of plant cells. J. Microsc. 135:147–158. http://dx.doi.org/10.1111/j.1365-2818.1984.tb00515.x.

Coetzee, J., Van der Merwe, C.F., 1986. The osmotic effect of glutaraldehyde-based fixatives on plant storage tissue. J. Microsc. 141:111–118. http://dx.doi.org/10.1111/j.1365-2818.1986.tb02705.x.

Costerton, J.W., Lewandowski, Z., Caldwell, D.E., Korber, D.R., Lappin-Scott, H.M., 1995. Microbial biofilms. Annu. Rev. Microbiol. 49, 711–745.

De Vrankrijker, A.M., van der Ent, C.K., van Berkhout, F.T., Stellato, R.K., Willems, R.K., Bonten, M.J., Wolfs, T.F., 2011. *Aspergillus fumigatus* colonization in cystic fibrosis: implications for lung function? Clin. Microbiol. Infect. 17 (9):1381–1386. http://dx.doi.org/10.1111/j.1469-0691.2010.03429.x.

Dierichs, R., 1979. Ruthenium red as a stain for electron microscopy. Some new aspects of its application and mode of action. Histochemistry 64 (2), 171–187.

Donlan, R.M., 2002. Biofilms: microbial life on surfaces. Emerg. Infect. Dis. 8 (9):881–890. http://dx.doi.org/10.3201/eid0809.020063.

Ferreira, J.A., Carr, J.H., Starling, C.E., de Resende, M.A., Donlan, R.M., 2009. Biofilm formation and effect of caspofungin on biofilm structure of *Candida* species bloodstream isolates. Antimicrob. Agents Chemother. 53:4377–4384. http://dx.doi.org/10.1128/AAC.00316-09 PMID: 19546368).

Ferreira, J.A.G., Penner, J.C., Moss, R.B., Haagensen, J.A.J., Clemons, K.V., Spormann, A.M., et al., 2015. Inhibition of Aspergillus fumigatus and its biofilm by Pseudomonas aeruginosa is dependent on the source, phenotype and growth conditions of the bacterium. PLoS ONE 10 (8):e0134692. http://dx.doi.org/10.1371/journal.pone.0134692.

Flemming, H.C., Neu, T.R., Wozniak, D.J., 2007. The EPS matrix: the "house of biofilm cells". J. Bacteriol. 189, 7945–7947.

Flemming, H.-C., Wingender, J., Szewzyk, U., Steinberg, P., Rice, S.A., Kjelleberg, S., 2016. Biofilms: an emergent form of bacterial life. Nat. Rev. Microbiol. 14:563–575. http://dx.doi.org/10.1038/nrmicro.2016.94.

Fox, E.P., Nobile, C.J., 2012. A sticky situation: untangling the transcriptional network controlling biofilm development in *Candida albicans*. Transcription 3, 315–322.

Gaylarde, P., Sarkany, I., 1968. Ruthenium tetroxide for fixing and staining cytoplasmic membranes. Science 161 (3846):1157–1158. http://dx.doi.org/10.1126/science.161.3846.1157.

Hayat, M.A., 2000. Principles and Techniques of Electron Microcopy, Biological Applications. fourth ed. Cambridge University Press, Cambridge, UK.

Joubert, L.-M., 2009. Visualization of hydrogels with variable pressure SEM. Microsc. Microanal. 15 (S2):1308–1309. http://dx.doi.org/10.1017/S1431927609096263.

Joubert, L.-M., 2012. VP-SEM: unsung hero of SEM imaging. Imaging Microsc. 2012:1–5 Dec, http://www.imaging-git.com/.

Joubert, L.-M., McDonald, K., 2016. SEM visualization of biological samples using Hitachi ionic liquid HILEM IL 1000: a comparative study. Microsc. Microanal. 22 (S3): 1170–1171. http://dx.doi.org/10.1017/S1431927616006693.

Joubert, L.-M., Ferreira, J.A.G., Stevens, D.A., Cegelski, L., 2015. *Aspergillus fumigatus* biofilms SEM: effect of processing techniques. Microsc. Microanal. 21 (S3):935–936. http://dx.doi.org/10.1017/S1431927615005474.

Kaur, S., Singh, S., 2014. Biofilm formation by *Aspergillus fumigatus*. Med. Mycol. 52 (1), 2–9.

Kojic, E.M., Darouiche, R.O., 2004. *Candida* infections of medical devices. Clin. Microbiol. Rev. 17, 255–267.

Lappin-Scott, H.S., Burton, S., Stoodley, P., 2014. Revealing a world of biofilms — the pioneering research of Bill Costerton. Nat. Rev. Microbiol. 12, 781–787.

Luft, J.H., 1971. Ruthenium red and violet. I. Chemistry, purification, methods of use for electron microscopy and mechanism of action. Anat. Red. 171, 347–368.

Manavathu, E.K., Vager, D.L., Vazquez, J.A., 2014. Development and antimicrobial susceptibility studies of in vitro monomicrobial and polymicrobial biofilm models with *Aspergillus fumigatus* and *Pseudomonas aeruginosa*. BMC Microbiol. 14, 53–67.

Mowat, E., Butcher, J., Lang, S., Williams, C., Ramage, G., 2007. Development of a simple model for studying the effects of antifungal agents on multicellular communities of *Aspergillus fumigatus*. J. Med. Microbiol. 56:1205–1212. http://dx.doi.org/10.1099/jmm.0.47247-0.

Muller, F.M., Seidler, M., Beauvais, A., 2011. *Aspergillus fumigatus* biofilms in the clinical setting. Med. Mycol. 49 (Suppl. 1):S96–S100. http://dx.doi.org/10.3109/13693786.2010.502190. Epub 2011.

Nobile, C.J., Johnson, A., 2015. *Candida albicans* biofilms and human disease. Annu. Rev. Microbiol. 69, 71–92.

Polke, M., Hube, B., Jacobsen, I.D., 2015. *Candida* survival strategies. Adv. Appl. Microbiol. 91, 139–235.

Porter, K.R., Kallman, F., 1953. The properties and effects of osmium tetroxide as a tissue fixative with special reference to its use for electron microscopy. Exp. Cell Res. 4 (1), 127–141.

Priester, J.H., Horst, A.M., Van de Werfhorst, L.C., Saleta, J.L., Mertes, L.A., Holden, P.A., 2007. Enhanced visualization of microbial biofilms by staining and environmental scanning electron microscopy. J. Microbiol. Methods 68, 577–587.

Reichhardt, C., Ferreira, J.A.G., Joubert, L.-M., Clemons, K.V., Stevens, D.A., Cegelski, L., 2015. Analysis of the *Aspergillus fumigatus* biofilm extracellular matrix by solid-state nuclear magnetic resonance spectroscopy. Eukaryot. Cell 14 (11):1064–1072. http://dx.doi.org/10.1128/EC.00050-15 (Epub 2015 Jul 10).

Reichhardt, C., Stevens, D.A., Cegelski, L., 2016. Fungal biofilm composition and opportunities in drug discovery. Future Med. Chem. 8:1455–1468. http://dx.doi.org/10.4155/fmc-2016-0049.

Reimann, B., 1961. Zur Verwendbarkeit von Rutheniumrot als elektronmikroskopisches Kontrastierungsmittel. Mikroskopie 16, 224–226.

Sakaue, M., Shiono, M., Konomi, M., Tomizawa, J., Nakazawa, E., Kawai, K., Kuwabata, S., 2014. New preparation methods using ionic liquid for fast and reliable SEM observation of biological specimens. Microsc. Microanal. 20 (S3):1012–2013. http://dx.doi.org/10.1017/S1431927614006783.

Santos, A.L.S., 2015. Biofilm: a robust and efficient barrier to antifungal chemotherapy. J. Antimicrob. 1:e101. http://dx.doi.org/10.4172/Antimicro.1000e101.

Speirs, J.J., Van der Ent, C.K., Beekman, J.M., 2012. Effects of *Aspergillus fumigatus* colonization on lung function in cystic fibrosis. Curr. Opin. Pulm. Med. 18, 632–638.

Trent, J.S., Scheinbeim, J.I., Couchman, P.R., 1983. Ruthenium tetraoxide staining of polymers for electron microscopy. Macromolecules 16, 589–598.

Villena, G.K., Fujikawa, T., Tsuyuma, S., Gutierrez-Correa, M., 2010. Structural analysis of biofilms and pellets of *Aspergillus niger* by confocal laser scanning microscopy and cryo scanning electron microscopy. Bioresour. Technol. 101, 1920–1926.

Voelker, D., Smejtek, P., 1996. Adsorption of ruthenium red to phospholipid membranes. Biophys. J. 70, 818–830.

Weber, K., Delben, J., Bromage, T.G., Duarte, S., 2014. Comparison for SEM and VPSEM imaging techniques with respect to *Streptococcus* mutants biofilm topography. FEMS Microbiol. Lett. 350, 175–179.

Weimer, P.J., Price, N.P., Kroukamp, O., Joubert, L.M., Wolfaardt, G.M., Van Zyl, W.H., 2006. Studies of the extracellular glycocalyx of the anaerobic cellulolytic bacterium *Ruminococcus albus* 7. Appl. Environ. Microbiol. 72, 7559–7566.

Wu, Y., Liang, J., Rensing, K., Chou, T.-M., Libera, M., 2014. Extracellular matrix reorganization during cryo preparation for Scanning Electron Microscope imaging of Staphylococcus aureus biofilms. Microsc. Microanal. 2014. 20 (5):1348–1355. http://dx.doi.org/10.1017/S143192761401277X.

Xiao, J., Klein, M.I., Falsetta, M.L., et al., 2012. The exopolysaccharide matrix modulates the interaction between 3D architecture and virulence of a mixed-species oral biofilm. PLoS Pathog. 8 (4):e1002623. http://dx.doi.org/10.1371/journal.ppat.1002623.

Yousif, A., Jamal, M.A., Raad, I., 2015. Biofilm-based central line-associated bloodstream infections. Adv. Exp. Med. Biol. 830, 157–179.